Optics of a Granular Imaging System (i.e. "Orbiting Rainbows")

Scott A. Basinger[*a], David Palacios[a], Marco B. Quadrelli[†a],
Grover A. Swartzlander Jr.[b]

[a]Jet Propulsion Laboratory, California Institute of Technology, 4800 Oak Grove Drive, Pasadena, CA 91109-8099
[b]Rochester Institute of Technology, One Lomb Drive, Rochester, NY 14623-5603

ABSTRACT

In this paper, we present some ideas regarding the optics and imaging aspects of *granular spacecraft*. Granular spacecraft are complex systems composed of a spatially disordered distribution of a large number of elements, for instance a cloud of grains in orbit. An example of this application is a spaceborne observatory for exoplanet imaging, where the primary collecting aperture is a cloud of small particles instead of a monolithic aperture.

Keywords: imaging system, dynamics, control, integrated modeling, granular media

1. INTRODUCTION

"Orbiting Rainbows" is a Phase II NASA Innovative Advanced Concepts (NIAC) study that is investigating the creation of a space-based observatory from granular media. The goal of this research is to identify ways to optically manipulate and maintain the shape of a cloud of dust-like matter so that it can function as an adaptive surface with useful electromagnetic characteristics in the optical or microwave bands. The investigators are developing a technology roadmap with the goal of constructing a very large and lightweight granular aperture by shaping a cloud of micron-sized particles. This "cloud optic" will be relatively simple to package, transport, and deploy. It is reconfigurable and can be re-targeted; the focal length is variable and it will be self-healing and ultimately disposable. With near-term plans to build 30 meter ground-based telescopes for astronomy, the demand for higher resolution optics in space continues to grow not only for exo-planet detection, but also for earth-based science, including hyper-spectral imaging and for monitoring of the oceans and land masses (e.g. seismic monitoring).

The useful engineering properties of a cloud of granular matter in space are virtually unknown. Granular matter is considered to be the fifth state of matter (after solid, liquid, gaseous, and plasma) by virtue of its peculiar response characteristics (cohesiveness, fluid behavior, compactification, phase transformation capability, and others). However, it is a fact that the dynamics, controllable properties, and consequent benefits of engineering and manipulating granular matter such as dust grains, powders, and granular spacecraft is poorly known to the space exploration community. Recent work[‡] has investigated the feasibility of granular imaging system, concluding that such a system could be built and controlled in orbit. A *granular spacecraft* has been defined[1] as a collection of a large number of space-borne elements (in the 1000s) designed and controlled such that a desirable collective behavior emerges, either from the interactions among neighboring grains, and/or between the grains and the environment.

Typically, the cost of an optical system is driven by the size and mass of the primary aperture. The solution that we propose[§] uses the nonlinear optical properties of a cloud of micron-sized particles to construct an optical system in space. The cloud of grains may be shaped into a specific surface by light pressure, allowing for the formation of a very large and lightweight optical system aperture, hence reducing overall mass and cost.

This concept, in which the aperture does not need to be continuous and monolithic, would increase the aperture size several times compared to large NASA space-borne observatories currently envisioned such as ATLAST, allowing for a

[*] Group Supervisor, Wavefront Sensing and Control, Mail Stop 306-451.
[†] Research Technologist and Group Lead, Mobility and Robotic Systems Section, Mail Stop 198-219

[§] http://www.nasa.gov/directorates/spacetech/niac/2012_phase_I_fellows_quadrelli.html#.VKx2ykvxVdB

UV/Optical/IR Space Telescopes and Instruments: Innovative Technologies and Concepts VII,
edited by Howard A. MacEwen, James B. Breckinridge, Proc. of SPIE Vol. 9602, 96020E
 · doi: 10.1117/12.2185699

true Terrestrial Planet Imager that would be able to resolve exo-planet details and do meaningful spectroscopy on distant worlds. To accomplish this goal, we need to investigate the conditions to manipulate and maintain the shape of an orbiting cloud of dust-like matter so that it can function as an ultra-lightweight surface with useful and adaptable electromagnetic characteristics. Consider the following scenario for a Granular Telescope: 1) the cloud is first released; 2) it is contained by laser pressure to avoid dissipation and disruption by gravitational tidal forces, 3) it is shaped by optical manipulation into a two-dimensional object (coarse control), and 4) ultimately into a surface with imaging characteristics (fine control). The cloud shape has to be maintained against orbital disturbances by continuous figure control, also achieved optically. Applying differential light pressure retargets the entire cloud, so that a change of the optical axis can be induced. Selected parts of the cloud are reshaped when required for wavefront control, thus enabling higher quality optics. The entire imaging system is now in full operation, as 5) a multilens system searching for exo-planets, or 6) as a radio receiver engaged in remote sensing investigations. The potential advantages of the granular spacecraft concept are that: a) it can result in an ultra-lightweight system, made of very simple, very low cost, units; b) it can be very big: the cloud can distribute itself to kilometer scales, without the need to fill the aperture; c) the cloud is easy to package, transport and deploy; d) it is reconfigurable, and can be retargeted and repointed with non-mechanical means; e) the cloud is a highly fault-tolerant system with very low vulnerability to impacts. Other potential advantages offered by the cloud properties as optical system involve possible combination of properties (combined transmit/receive), variable focal length, combined refractive and reflective lens designs, and hyper-spectral imaging.

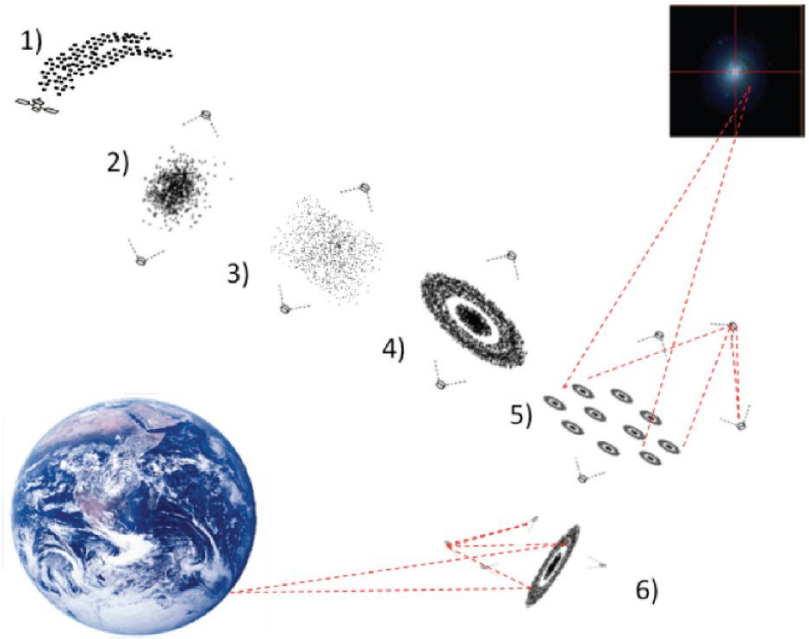

Figure 1. Sequence for Granular Telescope deployment and commissioning

2. THE GRANULAR IMAGER OPTICAL DESIGN

Reflective Optical Designs

We developed concepts for refractive, reflective and holographic systems and designed optical correction and collection systems. We designed an optical imaging system for multiple aerosol optics that combines several layers of sensing and control to adapt to possible misalignments and shape errors in the aerosol. The design also combines the light from several of these "clouds" to synthesize a large, multiple-aperture system to increase light throughput and resolution. A two-dimensional version that includes two separate Granular Telescope, is shown in Fig. 2. The entire system is represented in the diagram on the right. Starlight enters from the left, reflects off the two separate patches, and is slowly focused toward the formation-flying spacecraft that collects, corrects, and combines the light from individual patches to a single detector. The diagram on the left is an enlarged drawing of the separate spacecraft/optical "bench" that contains all the optics to perform line-of-sight and mid- to low-spatial frequency wavefront sensing and control for the optical

system. The sequence of optics is as follows: the starlight is focused by granular spacecraft optic "patch", creating a spherical wavefront. Light from all patches converges at an intermediate focus, which can be seen in the left side of Figure 2. The light reflects off secondary mirror (Gregorian) and the light from each patch is collimated.

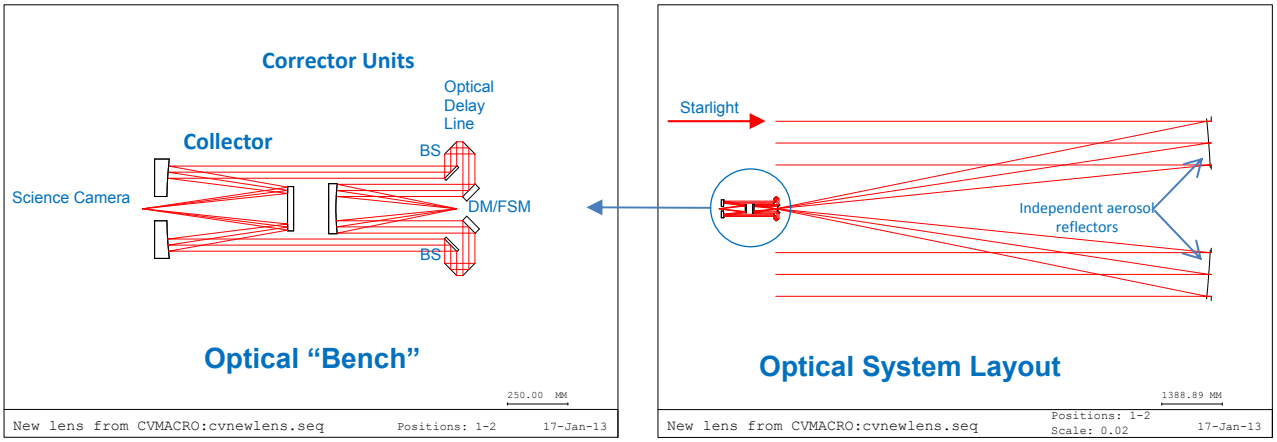

Figure 2. A two-dimensional slice of a multi-patch reflective system, with optical rays shown in red, is displayed on the right. An expanded view of the Optical "Bench" is displayed on the left

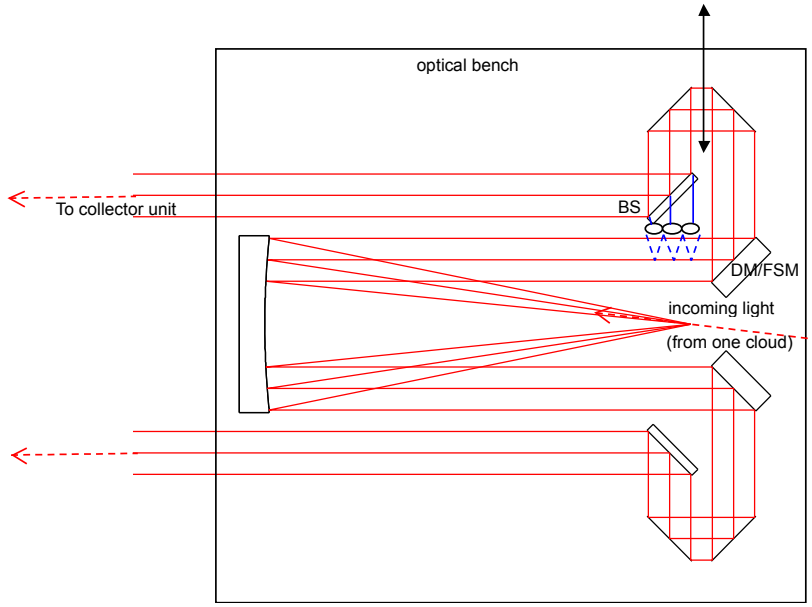

Figure 3. An expanded view of the corrector part of the optical "bench" that explicitly show the Shack-Hartmann wavefront sensor in blue. The SH sensor will be below the main optical path to avoid vignetting.

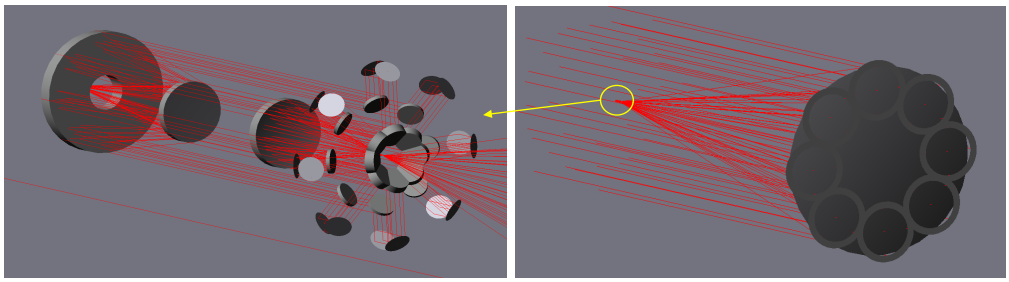

Figure 4. 3D solid optics view of the reflective imaging system concept design with 8 cloud patches forming the aperture.

The collimated light from each patch then continues to a separate adaptive optics system. A combined fast steering mirror and deformable mirror correct pointing and low to mid-spatial frequency aberrations. An optical delay line is used to correct phasing difference between the patches and enables Fourier transform spectroscopy. A beam-splitter is included to allow some of the light to go to a Shack-Hartmann sensor to measure aberrations in the system and provides a feedback mechanism to the deformable mirror. The Shack-Hartmann placement can be seen in Figure 3 in blue. The light continues to the collector system, which consists of a Cassegrain telescope that combines and focuses the light from all the patches onto the science detector. Figure 4 shows a 3D solid picture of the optics, including 8 optical "patches".

For this system, the selected approach for cloud management/sensing/control is multistage, with an outer stage for formation stabilization, and an inner stage for telescope wavefront sensing and correction, relegating fine adaptive optics to a deformable/fast steering mirror stage in the optical bench. The system's relative range/bearing sensing and metrology is based on virtual telescope formation flying, in which distributed relative sensing is accomplished using Ka-Band transceivers/patch antennas, and a centralized laser metrology system, relying on a single laser source on the main light-collecting spacecraft, while single reflecting target are on other free-flying elements except granular spacecraft.

For the reflective optical system, height variations of the optical surface must be less than $\lambda^2/\Delta\lambda$, where $\Delta\lambda$ is the bandwidth of light, to achieve meaningful imagery. Longer wavelengths (e.g. >10 um) and smaller optical bandwidths make this requirement achievable with micron-sized particles for the cloud. Creating and maintaining a perfectly continuous surface is not likely to be achieved using the techniques we are considering in our approach, therefore sophisticated image processing algorithms will be required to synthesize an astronomical image. For example, taking several short exposures and using speckle imaging techniques would allow for weaker tolerances on the reflective surface. Instead of correcting for atmospheric instabilities, as is typical for speckle imaging, we would correct for the small changes of the mirror surface due to particles being constantly in motion.[2,3] Multiframe blind deconvolution[4] is a related technique to process multiple imperfect images to obtain a better estimate of the object. Utilizing multiple clouds would be a natural extension that would be applicable to speckle interferometry and increase the effective resolution of the system inversely proportional to the separation of clouds.[5,6]

In addition to the techniques mentioned above, the addition of a diversity mechanism to the optical path would allow for phase diversity[7] techniques to be used. We plan to use a MEMS-based microshutter array as a programmable coded aperture in a pupil plane. Using optimized patterns in the coded aperture, and taking multiple images, would allow phase diversity to reconstruct the "phase" of our reflective surface as well as obtain an enhanced estimate of the "object".

Refractive Optical Designs

In addition to the system design we created for treating the cloud as reflective optical surface, we also designed an optical system for treating the cloud as a refractive optic, or lens, to maintain maximum flexibility of the cloud physics for future work. One such system design is shown below in Figure 5. The diagram on the left shows light from an object passing through a medium (our cloud). The cloud causes the light to come to a focus and is then relayed to our separated spacecraft that contains the rest of the optical system, shown on the diagram on the right. The corrector/collector design is identical to the reflective system. The solid optics view on the bottom left shows 8-apertures, each consisting of one aerosol optic, forming an equivalent lens. The solid optics view on the bottom right shows a three-dimensional view of the corrector/collector system.

Bruggeman Effective Medium

One approach for creating a refractive optic using aerosols is to assume very small particles dispersed evenly throughout a volume and use Bruggeman effective medium theory to compute the focusing power of the volume of particles. The containment mechanism of the particles could be as simple as a thin transparent bladder that is released and filled in space. Other approaches could include a laser containment system.

The following computations assume particles with a refractive index approximating that of glass, for example, $n = 1.5$. According to Bruggeman effective medium theory, the focal length is:

$$f = \frac{2R}{(n_e - 1)}$$

where

$$(n_e - 1) = \frac{3}{2} F \frac{(n^2 - 1)}{(n^2 + 2)}.$$

F is the fill fraction, and n is the refractive index of the particles.

If we have cloud of diameter $2R$ = 10 meters, a fill fraction of 10^{-3}, and particles with an index of refraction of n = 1.5 then the focal length of the cloud is f = 23 km. The f-number is $f/D = 2.3 \times 10^3$. The Airy disk ($1.22\lambda f/D$) is then 1.4 mm (at λ = 0.5 micrometers), where the camera pixels would ideally be about this size to have a reasonable Q. The f-number is inversely related to the fill fraction as can be seen from

$$f / D = f / 2R = \frac{1}{(n_e - 1)}.$$

The angular resolution (λ/D) is independent of the fill fraction. If n = 1.5 is replaced with n ≈ 1, the focal length tends toward infinity. This represents a very "slow" optical system, however, since our plan is to have a separate spacecraft to collect the li Figure 6. Diffractive Optical system chromatic corrector (courtesy M. Rud, JPL)

Diffractive Optical Design

Another application of our orbiting rainbow that we considered is to create a holographic, or diffractive, optic for our system. Projects such as DARPA's Membrane Optic Imager Real-Time Exploration (MOIRE) are striving to create a "Fresnel Lens" in space using a thin membrane. The goals of that program are similar to ours, to develop a space-based telescope with apertures larger than 10 meters. It would rely on a separate spacecraft for with a chromatic corrector. Laboratory demonstrations of a 50 cm class diffractive primary mirror with long f-numbers (f/50) have been published[8]. Lawrence Livermore National Laboratory, through the "Eyeglass" program, has created a 5 meter diameter f/50 transmissive diffractive optic composed of 50 cm segments[9].

Palmer[10] considered using the nonlinear optical index of glass beads or aerosol droplets to organize the particles and trap them into Fresnel-like three-dimensional holographic gratings. Extrapolating from this concept, we have designed a third optical system that has a diffractive optical element (DOE) as its primary lens. The system design is nearly identical to the other two systems we designed, but with the primary optics replaced by a thin holographic lens.

A diffractive lens is inherently monochromatic, it only brings light to a focus for the wavelength it was designed for. However, it is straightforward to design an all-refractive chromatic correction system that provides a diffraction limited system with a 10% bandwidth. Meinel and Meinel published a basic design for such a system[11,12]. M. Rud at JPL created the design pictured below (Fig. 6) for a concept for the MOIRE project. More complex correctors that include a reverse Fresnel lens have also been proposed for space telescope applications[13].

Characteristic	Reflective	Refractive	Diffractive
Each particle needs to be precision controlled	Yes	No	Yes
Optical Bandwidth	Very high	Constrained	Very constrained

Table 1 Comparison of three optical systems

Expected Technology Developments

One developing technology we have assumed will continue to improve is fast steering mirrors that are also deformable mirrors. This is used to control both line-of-sight errors in our system and high-spatial frequency errors caused by thermal fluctuations in the cloud of particles. Northrop Grumman's AOA Xinetics is actively developing such mirrors and we can expect they will improve in control authority and number of actuators as our Orbiting Rainbows concept proceeds.

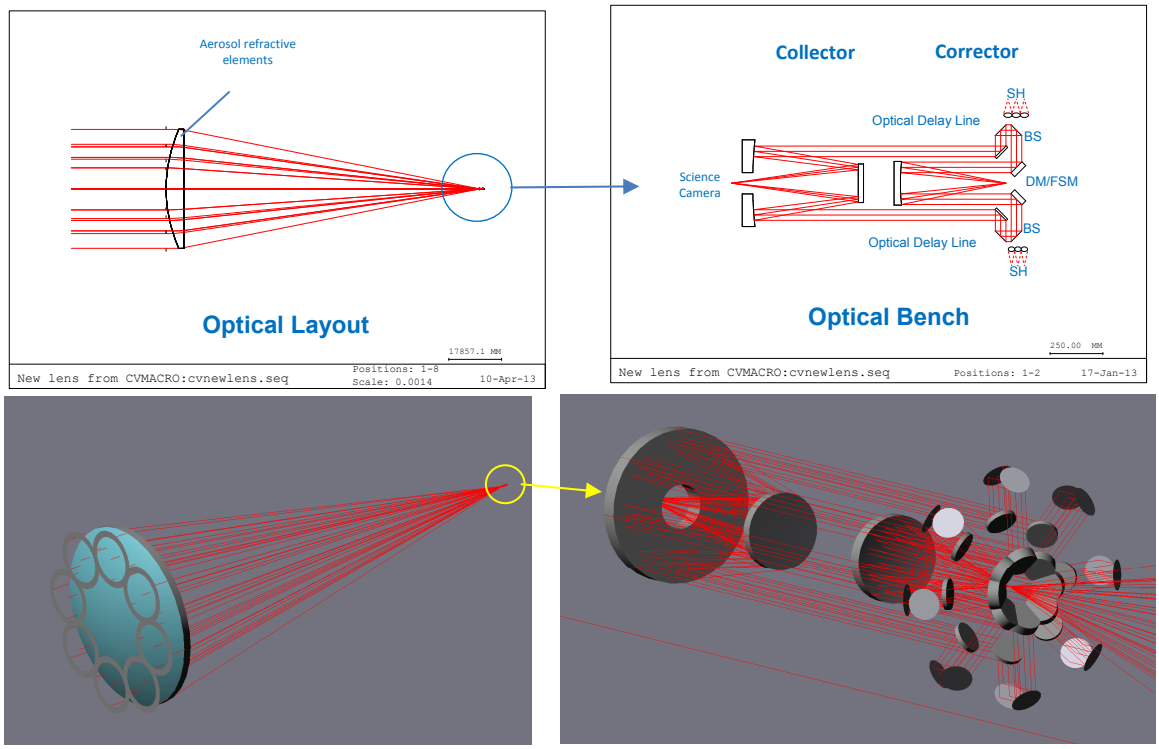

Figure 5. Refractive optical system design, both 2-D and solid optics views.

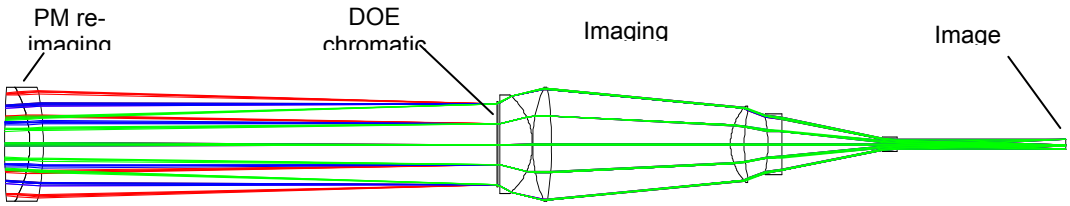

Figure 6. Diffractive Optical system chromatic corrector

Metric	Conventional Mirror SoA	Light-Weight Mirror SoA	Aerosol Objective
Mass Areal Density	40-100 kg/m2	10-20 kg/m2	<1 g/m2
Surface Figure Error	10 nm RMS	14 nm RMS	100 nm RMS
Surface microroughness	<5Å	<10Å	<100Å
Size	0.1 to 2.4m and larger	0.3 to 1.35m and larger	1 to 10m
Deployable	No	No	Yes
Thermal stability	Low CTE	Thermally controlled	TBD

Table 2 Comparison to State of Art

The fields of computational optics, wavefront sensing and control, and computational photography continue to develop at a rapid pace. Although our project has shown initial success with imaging a simulated binary star system through a fully-filled, glitter realization of our Orbiting Rainbows concept, we welcome further advances to reduce the stringent requirements placed on our particle-based mirrors. Since we plan to combine data from multiple images, "Lucky Imaging" is one technology that will help us address image estimation.

3. EXO-PLANET MEASUREMENT REQUIREMENTS

This paper makes extensive use of the Exo-C STDT Final Report (2014). The work accomplished by the Exo-C mission concept study is leveraged to quickly derive system requirements to achieve a similar mission. The direct detection of exo-planets requires an imaging system to be able to detect the faint reflected light from the exo-planet while not being blinded by the glare of the parent star the planet orbits. This places stringent requirements on the system to be able to suppress the light from the parent star while leaving the light from the exo-planet intact. For example, as seen from outside our solar system, the brightness of Jupiter at quadrature is given by, $B=1/4\ (\text{albedo})\cdot(R\_J/(5.2\ \text{AU}))^2 \cong 10^{-9}$ and detection of an Earth like planet would require starlight suppression on the order of 10^{-10}. Of course it is not enough to just suppress the starlight, you must also maintain starlight suppression stability over the time of a measurement. Otherwise, you signal will be contaminated with stellar light and your contrast will degrade. Exo-planets with stellar contrasts of 10^{-9} will have brightness in the range of V=23-29, with a median of V=27. Therefore depending on the collection area of the imaging system, the integration time may be on the order of multiple days. As a point of reference, the recent Exo-C mission study report quoted integration times of 10 days to spectrally characterize a planet for that system's $3m^2$ collecting area.

The spatial field of view (FOV) is the area around a star where planets may be visible to our imaging system as depicted in Fig. 7. The spatial FOV is defined by two angular measurements: the inner and outer working angles. The inner working angle (IWA) defines how close to a parent star you can see the planet at the required contrasts stated above. The IWA is limited by the imaging system's resolving power and the control bandwidth of an imaging systems starlight suppression system. The outer working angle (OWA) defines how far away from a parent star you can see a planet at or above the required contrast. The OWA is typically limited by the control bandwidth of an imaging system's starlight suppression system. For an ideal perfect imaging system the OWA is limited by the detector's FOV. The EXO-C mission study report quoted a desired IWA of 0.26" at 900nm (0.16" at 550 nm) and a desired OWA of 1.4" at 900nm.

After detecting an exo-planet, it will be highly desirable to characterize the spectral features of the exo-planet's signal. Detailed spectral analysis of an exo-planet can be used to determine if a planet has an atmosphere or not. If the exo-planet does have an atmosphere, spectral analysis may enable us to determine the composition of the atmosphere as well. In the previously mentioned Exo-C mission study report, it was determined that to achieve exo-planet characterization a wavelength range of 0.45-1.0μm was desired. This range encompasses several absorption features that are characteristic to molecules needed to support life. They also determined that Exo-planet characterization requires fine spectral sampling to discern features in the spectra. a spectral resolving power of, R~70 was required to achieve exo-planet characterization. Achieving a spectral resolving power of R~70 requires the system to maintain a decent signal to noise (SNR) over spectral elements on the order of SNR ~10.

4. A WAVE-FRONT CONTROL ARCHITECTURE FOR A GRANULAR IMAGER

A granular imager is a space-borne imaging system that makes use of a collection of small reflective grains to form a sparsely filled primary mirror. The concept is depicted graphically in Fig. 8, where a cloud of reflective grains is constrained by a space-borne optical trap into the parabolic shape of a primary mirror. Light reflected from each grain is then focused into a back-end system consisting of a control system and detector. However, to be an effective imager with a useful point spread function, the wavefronts reflected from the parabolic surface of the cloud must be corrected. This section details a control system that may be used in conjunction with the optical trapping system to correct the wave-fronts so that the granular imager will generate high resolution image that fully realize the potential of larger aperture sizes.

The challenge of a wavefront control system for a granular imager is to correct for the scattered speckle field when the effective surface roughness of the granular media is on the order of μm. It is unlikely that a single deformable optic will have both the range and control accuracy to correct for such roughness. Therefore, we opted for a staged control architecture as depicted in Fig 9.

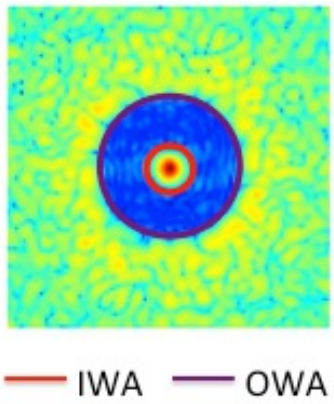

Figure 7. Coronagraph FOV

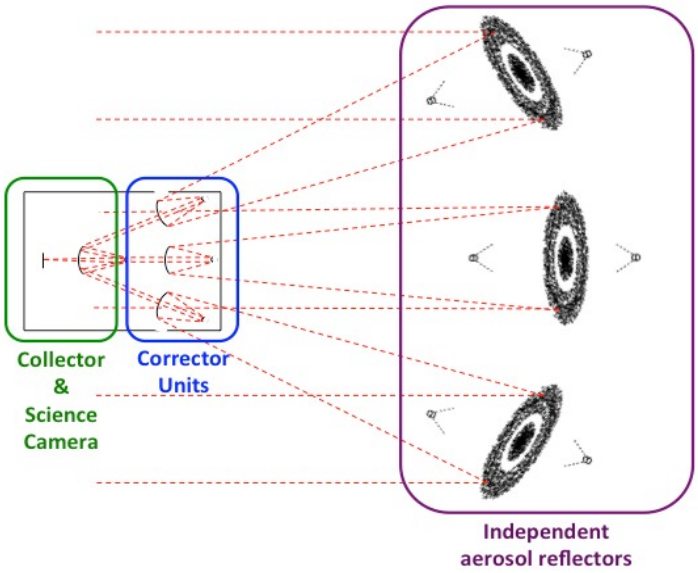

Figure 8 Granular Imager multi-aperture concept

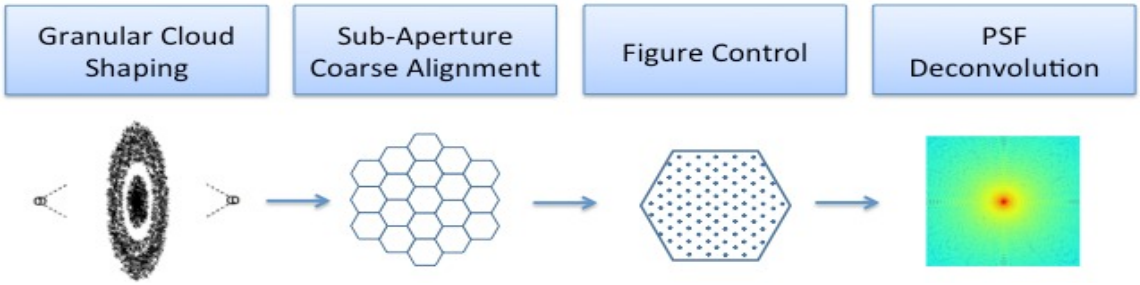

Figure 9. Wavefront Control Architecture

The wavefront control process follows the steps outlined below:

1. **Granular Cloud Shaping** – Grains are trapped in an optical trap, where they are shaped into a parabola
2. **Sub Aperture Coarse Alignment** – The trapped grains may be broken into regions or sub-apertures. Correcting for coarse misalignments between sub-apertures, corrects the low spatial frequency surface roughness of our granular imager, thereby making the PSF of the granular imager more compact.
3. **Figure Control** – Now that each sub-aperture is controlled globally with respect to each other, we can control the figure of each sub-aperture.
4. **Computational Imaging**. A combination of PSF deconvolution techniques and computational imaging will be used to compensate for less-than-ideal imaging as a result of the granular nature of the primary mirror.

An optical design that implements the above described wavefront control architecture is depicted in Fig. 3. In this design, the cloud of grains is re-imaged onto an array of fast steering deformable mirrors (DM/FSM). The tip/tilt of each cloud sub-aperture are controlled so that the entire collections of clouds fit onto a curved surface. A Shack-Hartmann wavefront sensor is used to sense the figure error that the DM/FSM must correct. In addition, there is an optical delay line that can be used to phase multiple granular telescopes together as a hybrid segmented granular imager design as depicted in Fig.4.

To detect exoplanets requires near perfect optical systems that are figure controlled to the sub-nanometer level. To achieve this goal one must have excellent control hardware but also must employ control algorithms that can command

the control system appropriately. The development of wavefront control algorithms that can meet such demand is a topic of intense research. In 2007, Give'on et al[14] proposed a general correction methodology called electric field conjugation (EFC) to control a coronagraph's residual scattered speckle field. This technique is applicable to a granular imager because it is a method for controlling coherent scatter, which we know will be the limiting factor on performance. With EFC the electric field in an image plane is corrected by applying the conjugate electric field as the correction, as opposed to phase conjugation techniques that try to correct for phase errors in the pupil plane[15]. The EFC correction process is outlined in Fig. 10. The most challenging aspect of the control process is the inversion of the G matrix, where several techniques have been proposed[14].

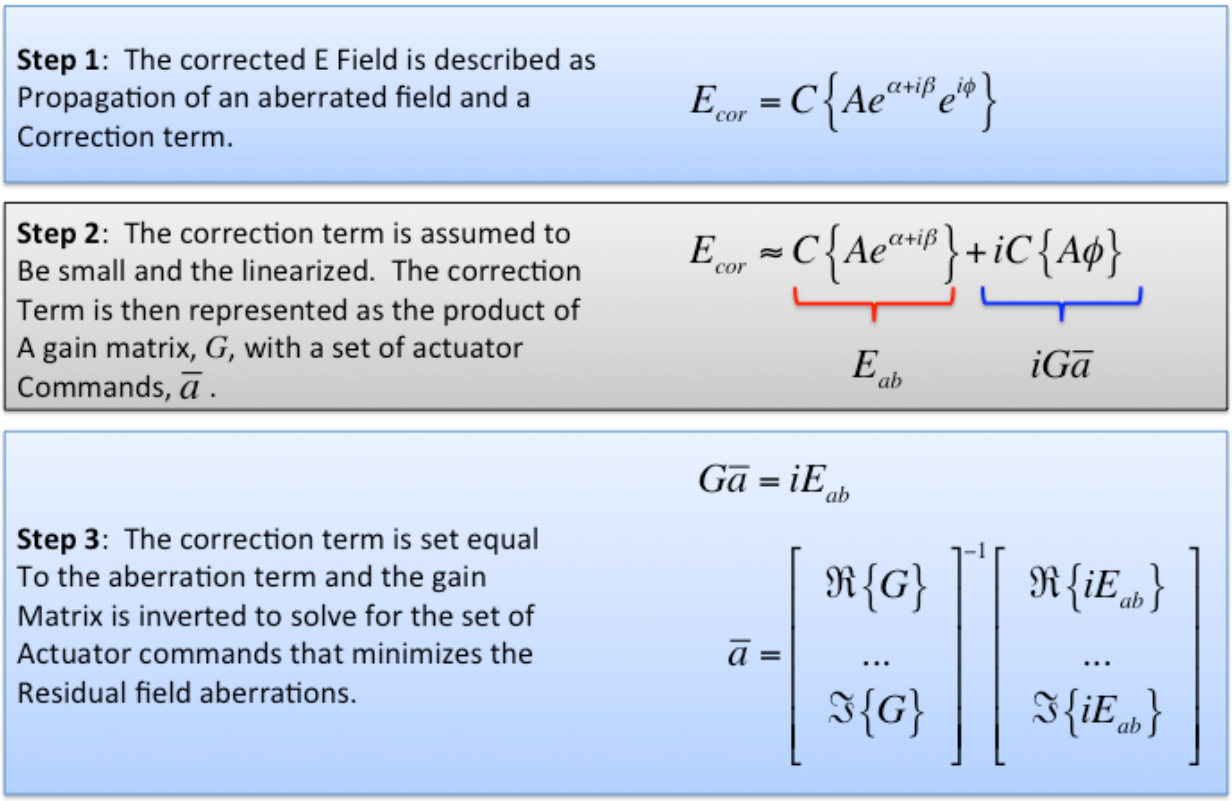

Figure 10. Electric Field Conjugation Correction

We may also use EFC to sense the electric field in the image plane by using the conjugate field as a method to probe the wavefront. Give'on et al[14] demonstrated that it is possible to derive the electric field in the image plane by applying sets of opposite probe patterns as depicted in Fig. 11. An example of a set of probe patterns and their responses are depicted in Fig. 12 and Fig. 13, respectively. The estimated image plane electric field is compared to the actual field in Fig. 14.

By Setting the DM in pairs of opposite patterns the real and imaginary components of the pupil aberrations may be determined without the use of a separate wave front sensor. This is highly desirable for low-light imaging

$$I_{probe} \approx \left| E_{ab} + iC\left\{A\varphi_{probe}\right\} \right|^2$$

$$\begin{bmatrix} \Re\{E_{ab}\} \\ \Im\{E_{ab}\} \end{bmatrix} = \frac{1}{4} \begin{bmatrix} \Re\{iC\{A\varphi_1\}\} & \Im\{iC\{A\varphi_1\}\} \\ \vdots & \vdots \\ \Re\{iC\{A\varphi_k\}\} & \Im\{iC\{A\varphi_1\}\} \end{bmatrix} \begin{bmatrix} I_1^+ - I_1^- \\ \vdots \\ I_k^+ - I_k^- \end{bmatrix}$$

Figure 11. EFC Probing

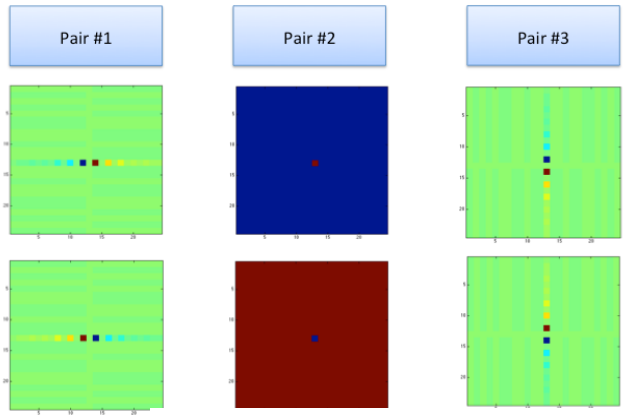

Figure 12. EFC Probe Patterns

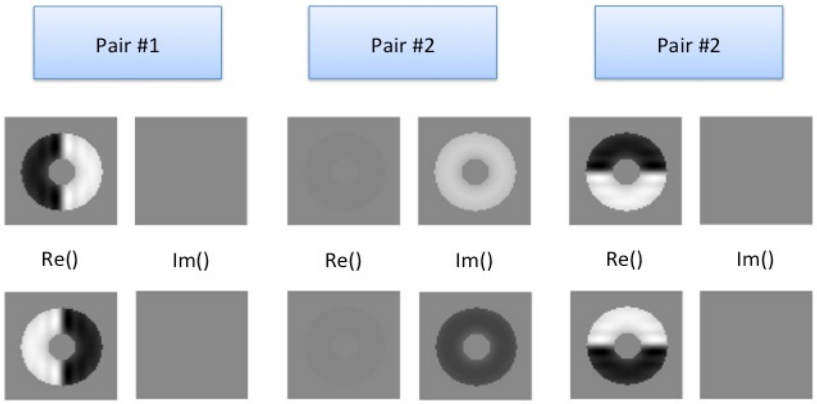

Figure 13. EFC Probe Responses

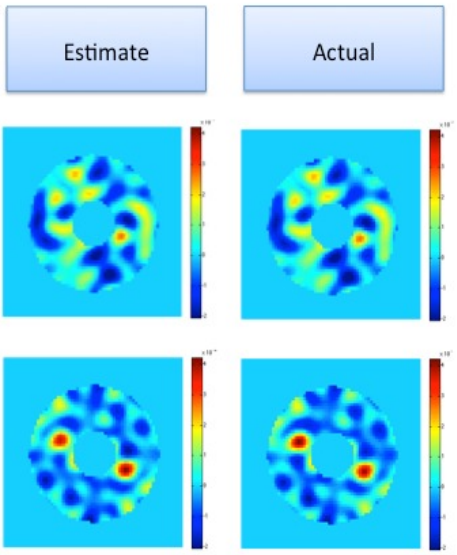

Figure 14. Comparison of the actual and estimated pupil fields.

Wavefront Sensing

Wavefront Sensing (WFS) is the measurement of the overall effect of the optical aberrations in an imaging system, such as a space telescope. Phase Retrieval is an image-based WFS tool, taking as its input data defocused images of an unresolved object such as a star or an optical pinhole or fiber. It computes a WF map – a 2-dimensional array of Optical Path Difference values – showing the deviation of the actual wavefront from its spherical ideal. For telescopes equipped with actuated optics, such as deformable or movable mirrors, this WF map provides the information needed for control of WF errors, and it does so in the actual science cameras, without requiring a dedicated WFS instrument

Phase Diversity is a superset of Phase Retrieval that attempts not only to estimate phase errors in a system, but also the object that forms an image. Therefore, it is not limited to an unresolved point source, but utilizes an extended scene. There are many methods for performing phase diversity, one of which, multiframe blind deconvolution, is described in detail in the following section.

Shack-Hartman wavefront sensing utilizes a dedicated instrument, which includes a lenslet array at a pupil to convert wavefront slope to centroid offsets on a separate detector. Therefore, part of the light from the science path must be "picked off", typically using a beamsplitter, for this instrument. The advantage of a Shack-Hartman wavefront sensor is that is has a relatively high dynamic capture range and the image processing requirements are low. Therefore is can make rapid phase estimates (typical systems run at 500 Hz or greater, including corrections on a deformable mirror). However, the spatial frequencies that it can measure are limited to the number of lenslets and it does not work across discontinuities, such as a segmented telescope system will have. Our system is not segmented, and therefore we will utilized this kind of wavefront sensor to interrogate and keep aligned individual aerosol clouds. When combining imagery from multiple apertures, or clouds, we plan to investigate using phase diversity.

Multiframe Blind Deconvolution

Technique such as "blind deconvolution"[16] are used if the diversity terms between images is not known or not well known. Multi-frame Blind Deconvolution[17] was developed for speckle imaging, where a precise measurement of a stellar object from the ground is not possible due to the changing index of refraction caused by the Earth's atmosphere. Schulz developed the technique for ground-based imaging of finite extent objects and Van Kampen and Paxman extended the technique to infinite extent objects, or objects that extend beyond the field of view[18].

In general, multi-frame blind deconvolution works by taking multiple images through the optical system. Ground-based techniques assume that the effect of the atmospheric effects are not known exactly, or not measured. However, certain information, such as measuring the Fried parameter (r_0) and relying on Kolmogorov statistics, are used in the algorithm. Recent work[19] has shown that high-order aberrations can be estimated and compensated for computationally. In our Phase 2 work, we simulated the cloud physics, and explored using multi-frame blind deconvolution to determine the quality of imagery that can be reconstructed using these advanced computational optics techniques. Another form of diversity that can be exploited for post-processing of multiple images to better estimate the object is wavelength diversity. This was discussed by Gonsalves[20] and a blind-image deconvolution approach was developed and tested more recently by Ingelby et al[21]. Assuming our system is polychromatic, we plan to pursue this technique as well.

5. GRANULAR IMAGER WFS&C SYSTEM PERFORMANCE

In this section, we examine the optical imaging performance of a granular imager for two types of systems: a high-resolution imager and a high-contrast coronagraph. The first system is depicted graphically in Fig 15. In this case the most important metric of performance is resolution. The modulation transfer function measures how the modulation of a sinusoidal intensity variation in the image plane will vary as a function of spatial frequency. An ideal system will pass the zeroth spatial frequency perfectly but the modulation slowly decreases with spatial frequency until it reaches the cutoff frequency, 2*Nyquist Rate, where the modulation falls to zero. Traditionally, an object is considered resolvable if it modulates the intensity by greater than 10%. It has also been shown that low contrast images are able to be boosted back to nominal using a Wiener filter as long as the signal to noise (SNR) of the system is sufficiently high[22], which often correlates with a 10% spatial frequency cutoff.

In the simulations presented in this section, the parabolic primary mirror of the granular imager was filled randomly with small, unresolved grains (grain size << granular imager focal length). The fill factor, or the fraction of the aperture that is filled with grains, was allowed to vary from 0.2 to 1.0. In addition, the wavefront phase aberrations were allowed to vary from 0 – 1 waves of rms error.

In the first simulation, the fill factor of the granular imager is allowed to vary but the wavefront phase had no phase aberrations in the pupil (0 waves rms). Fig. 16 is a plot of the granular imager MTF vs. spatial frequency for several fill factor values. As expected the modulation decreases as a function of fill factor. However the resolution doesn't change appreciably until the fill factor is below 0.3. The 10% resolution cutoff for a perfect system occurs at approximately 1.6*Nyquist rate, even with a fill factor of 0.4, the resolution cutoff has only degraded to 1.4*Nyquist or approximately 12%. Although the contrast suffers as we decrease the fill factor, we may still be able to recover ~90% of the image in post processing using standard Wiener filtering techniques.

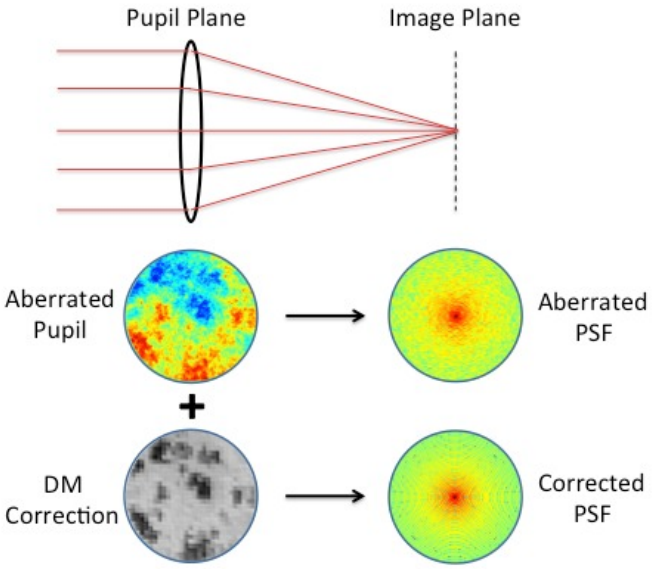

Figure 15. High-resolution imager with WFS&C system.

In the second simulation, the fill factor of the granular imager is now kept constant at fill factor = 1.0 and wavefront phase error (WFE) was allowed to be vary from 0.1 – 0.5 waves rms aberration. Fig. 17 is a plot of the granular imager MTF vs. spatial frequency for several WFE cases. These plots reveal, that even with a fully filled aperture, the WFE limits the performance of the system severely when the WFE is greater than approximately 0.2 waves. Therefore, it's important to correct the optical figure at least to this level for high-resolution imaging.

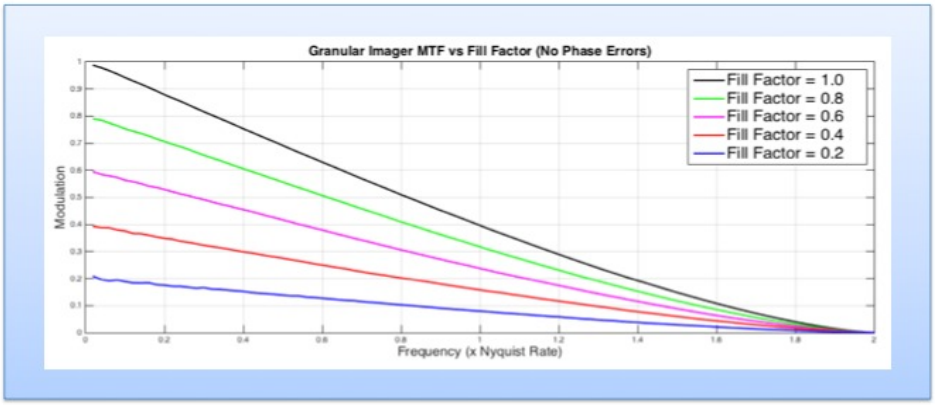

Figure 16. Granular Imager MTF vs. Fill Factor

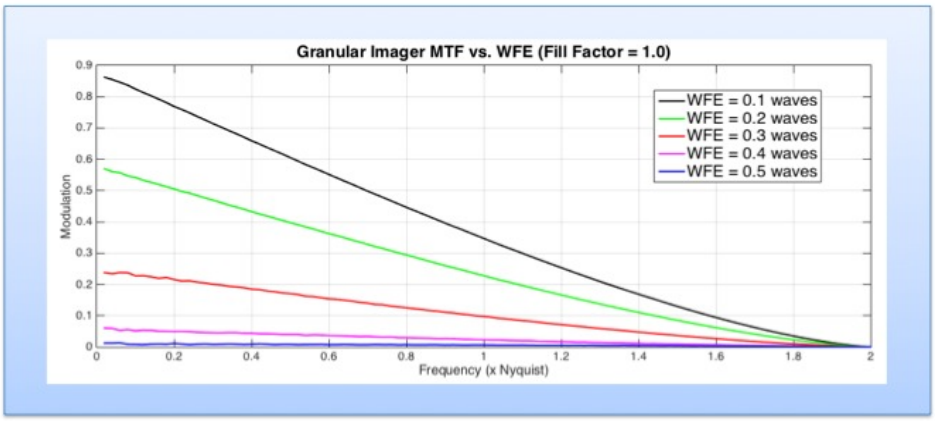

Figure 17. Granular Imager MTF vs. WFE

Contrast Analysis

High Contrast coronagraphy is a more challenging case for the granular imager and the wavefront control system is critical. The granular imager was modeled in conjunction with a hybrid Lyot coronagraph (HLC)[23] as depicted in Fig 18. In the results presented here, the grains were small, unresolved spheres that scattered light equally in all directions and the entrance pupil limited the surface roughness of the coronagraph to a simple power law power spectral density function with an peak-to-valley phase error of 200nm (30 nm rms), and an amplitude uniformity error of 8% peak-to-valley (1.2% rms). The coronagraph acts as a high-pass spatial filter, suppressing the light from an on-axis star, but leaves the light from nearby objects such as planets relatively intact. The difficulty of using a granular imager for this application lies in the fact that the grains will scatter light from the star into the mid-spatial frequencies where they will drown out the light from nearby objects, rendering the coronagraph ineffective. However, the use of a wavefront control system can help mitigate this issue. A wavefront control system was placed before the entrance aperture of the coronagraph as shown in Fig 19. In this configuration, two deformable mirrors (DM1 & DM2) are used to control the electric field at the occulter. One is placed in a pupil plane and another is placed outside the pupil plane. At least two DMs are required because a single DM located at the Coronagraph pupil could not control both phase and amplitude errors originating in the same plane simultaneously.

Contrast is a measure of how much the light from the on-axis star has been reduced as compared to nearby objects. The greater the contrast, the fainter an object can be and still be detected. Simulations of the contrast provided by the system above were run for a fill factor of 1.0 (normal aperture) and a fill factor of 0.5 (sparse aperture) are shown in Fig 20. As we expect when the fill factor is reduced from 1.0 to 0.5, light is scattered in all directions to form a speckle field. Note that in the normal aperture case (fill factor = 1.0) the scattered light rolls off as a power law as we defined it. However in the sparsely filled case (fill factor = 0.5) the light is scattered in all directions as expected. The control system allows us to dig a dark hole in the scattered light as shown in the zoomed in insets in the lower half of Fig 20. Although the contrast in the dark hole has decreased from 10^{-10} to 10^{-8}, we are still able to control the majority of the scattered light from the grains using the EFC algorithm in conjunction with two deformable mirrors (DM). If the wavefront control system were not able to control the scattered light, no dark hole would form. Two DMs gives you more controllability than one because we are increasing the number of degrees of freedom that we can use to control each point in the image plane. Therefore, it may be possible to increase the contrast by increasing the number of DMs used.

Now we ask the question: How sparse can an aperture be before we lose all controllability? To answer the question for the case of 2 DMs, we performed simulations where the fill factor was allowed to vary from 0.1 to 1.0. The mean contrast in the dark hole was plotted as a function of fill factor in Fig 21. As can be seen, the contrast in the dark hole increases for fill factors greater than 0.3 regardless of whether or not phase errors were present. This suggests that the granular cloud does not have to be perfectly shaped into a parabola but rather just needs to be shaped with an RMS surface roughness that is within the capture range of the wavefront control system. This allows one to trade between grain trapping error and the wavefront control capture range.

6. CONCLUSION

In this paper, we presented some ideas regarding the optics and imaging aspects of a *granular spacecraft*. Granular spacecraft are complex systems composed of a spatially disordered distribution of a large number of elements, for instance a cloud of grains in orbit. An example of application is a spaceborne observatory for exoplanet imaging, where the primary aperture is a cloud instead of a monolithic aperture. The application considered so far was a reflective imaging system for astrophysics, but many unexplored applications of granular spacecraft are yet to be discovered.

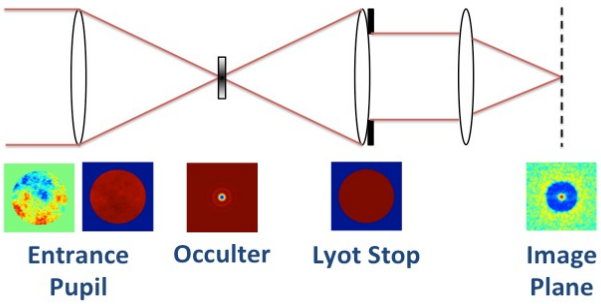

Figure 18. Hybrid Lyot Coronagraph

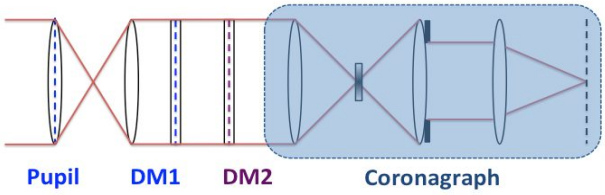

Figure 19. HLC Control System Architecture

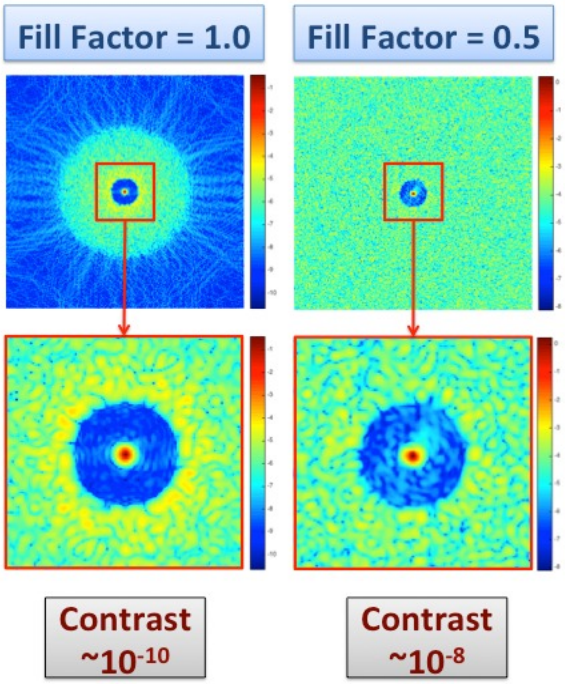

Figure 20. Granular Imager HLC Contrast vs Fill Factor.

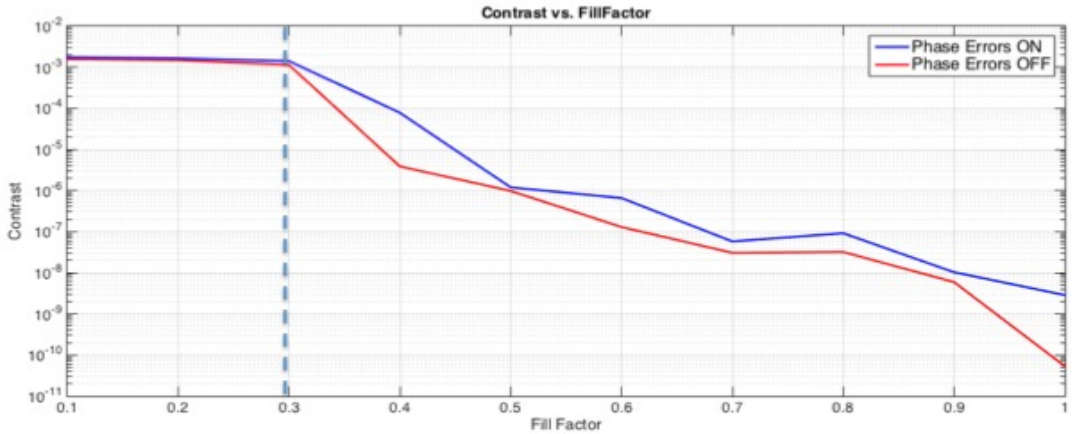

Figure 21. Granular Imager HLC Contrast vs. Fill Factor

ACKNOWLEDGMENTS

We would like to acknowledge XiaoPeng Peng and Alexandra Artusio, graduate students of Professor Swartzlander at the Rochester Institute of Technology, for their contributions towards advancing the practical demonstrations and modeling of granular imagers. We would also like to acknowledge Dr. Darmin D. Arumugam of the Jet Propulsion Laboratory, for his expansion of the granular image concept to radar frequencies.

This research was carried out at the Jet Propulsion Laboratory, California Institute of Technology, under a contract with the National Aeronautic and Space Administration under the NASA Innovative Advanced Concepts Program.

REFERENCES

[1] Quadrelli, M., Basinger, S., Swartzlander, G.: "Dynamics and Control of a Disordered System In Space," AIAA SPACE Conference, San Diego, CA, (2013).
[2] Labeyrie, A., "Attainment of Diffraction-Limited Resolution in Large Telescopes by Fourier Analysing Speckle Patterns in Star Images," Astron. Astrophy. **6**, 85 (1970).
[3] Beavers, W.I., Dudgeon, D.E., Beletic, J.W., and Lane, M.T., "Speckle Imaging through the Atmosphere," The Lincoln Laboratory Journal **2,** Number 2 (1989).
[4] Ayers, G.R., Dainty, J.C., "Iterative blind deconvolution method and its applications," Optics Letters **13,** No. 7 (1988)
[5] Weigelt, Gerd, "Modified astronomical speckle interferometry 'speckle masking'," Optical Communications **21,** (1) 55 (1977).
[6] Fienup, J.R. and Feldkamp, G.B., "Astronomical Imaging By Processing Stellar Speckle Interferometry Data," Proc SPIE 243, (1980).
[7] Paxman, R.G., Schulz, T.J. and Fienup, J.R., "Joint estimation of object and aberrations by using phase diversity," J. Opt. Soc. Am. A **9**, No. 7 (1992).
[8] Barton, I.M., Britten, J.A., Dixit, S.N., Summers, L.J., Thomas, I.M., Rushford, M.C., Lu, K., Hyde, R.A. and Perry, M.D., "Fabrication of large-aperture lightweight diffractive lenses for use in space," Applied Optics **40**(4), 447-451 (2001).
[9] Hyde, R.A., "Eyeglass: Large Aperture, Lightweight Space Optics," LLNL Report UCRL-ID-151390, (2003).
[10] Palmer, A.J., "Aerosol Lens," J. Optical Society of America **73**, 1568 ff (1983).
[11] Meinel, A.B. and Meinel, M.P., "Large membrane space optics: Imagery and aberrations of diffractive and holographic achromatized elements of high diffraction order," Opt Eng **41**(8), 1995-2007 (2002).
[12] Meinel, A.B. and Meinel, M.P, "Parametric dependencies of high-diffraction-order achromatized aplanatic configuration that employ circular or cross-linear diffractive optcal elements," AO **41**(34), 7155-7166 (2002).
[13] Lo, A.S. and Arenberg, J., "Architectures for space astronomical telescopes using Fresnel optics," *Proc. SPIE 6265*, Space Telescopes and Instrumentation I, (2006).
[14] Give'on, A. et al., "Broadband wavefront correction algorithm for high-contrast imaging systems," Proc. SPIE 6691, (2007).
[15] Give'on, A., Kasdin N.J., Vanderbei R.J., and Avitzour Y., "On representing and correcting wavefront errors in high-contrast imaging systems," JOSA A **23,** (2006).
[16] Kundur, D. and Hatzinakos, D., "Blind Image Deconvolution," IEEE Signal Process. Mag. **13**, 43-64 (1996).
[17] Schulz, T.J., "Multiframe blind deconvolution of astronomical images," J. Opt. Soc. Am A **10**, 1064-1073, (1993).
[18] van Kampen, W. and Paxman, R.G., "Multi-Frame Blind Deconvolution of Infinite-Extent Objects," Proc. SPIE 3433, Propogation and imaging through the Atmosphere II (1998).
[19] Scharmer, G.B., Lofdahl, M.G., van Werkhoven, T.I.M. de la Cruz Rodriguex, J., "High-order aberration compensation with multi-frame blind deconvolution and phase diversity image restoration techniques," A&A **521,** (2010).
[20] Gonsalves, R.A., "Phase retrieval and diversity in adaptive optics," Opt. Eng. **21**, 829-832 (1982).
[21] Ingleby, H.R. and McGaughey, D.R., "Real data results with wavelength-diverse blind deconvolution," Opt. Lett. **30,** No. 5, 489-491 (2005).
[22] Pratt, W.K., "Generalized Wiener Filtering Computation Techniques," IEEE Trans. on computers **c-21** (7), (1972).
[23] Trauger, J., Moody, D. and Gordon, B., "Complex apodized Lyot coronagraph for exoplanet imaging with partially obscured telescope apertures," Proc. SPIE 8864, (2013).